Contract No.:

This manuscript has been authored by Battelle Savannah River Alliance (BSRA), LLC under Contract No. 89303321CEM000080 with the U.S. Department of Energy (DOE) Office of Environmental Management (EM).

Disclaimer:

The United States Government retains and the publisher, by accepting this article for publication, acknowledges that the United States Government retains a non-exclusive, paid-up, irrevocable, worldwide license to publish or reproduce the published form of this work, or allow others to do so, for United States Government purposes.

Methyl Carbamate-Lithium Salt Deep Eutectic Electrolyte for Lithium-Ion Batteries

Dr. Nathaniel Z. Hardina,*, Dr. Zachary Ducaa, Dr. Adam Imelb, Dr. Patrick A. Warda,*

[a] N. Z. Hardin*, Z. Duca, P. Ward*

Advanced Manufacturing and Energy Science

Savannah River National Laboratory

Aiken, SC 29803 USA

E-mail: Nathaniel.Hardin@srnl.doe.gov

Patrick.Ward@srnl.doe.gov

[b] A. Imel Department of Chemical and Biomolecular Engineering

University of Tennessee Knoxville, Knoxville, TN 37996 USA

Supporting information for this article is given via a link at the end of the document.

Abstract: Deep eutectic electrolytes (DEEs) represent a burgeoning field in electrolytes for energy storage applications. Compared to the more conventionally studied Li-ion electrolyte systems, these electrolytes offer numerous advantages, such as high ion concentration, costs, lower temperature operation, and safety. In this work, we report the formation of a novel eutectic electrolyte based on lithium salts and methyl carbamate. These DEEs were formed via mixing lithium salts and low-cost methyl carbamate at ratios varying from 1:2 to 1:5 (mol:mol). The DEE formed from methyl carbamate and lithium hexafluorophosphate (LiPF6) at a 1:5 molar ratio generated a 4V stability window and a 25°C conductivity of up to 3.16E-3 S•cm-1. The DEE formed from methyl carbamate and lithium bis(trifluoromethane)sulfonimide (LiTFSI) at a 1:5 molar ratio generated a 3.2 V stability window and a 25°C conductivity of up to 2.87E-3 S•cm-1. The LiPF6 DEE also demonstrated a discharge capacity of 128 mAh•g-1after 50 cycles with 93% discharge capacity retention at moderate cycling rates of 0.5C in a lithium titanate (LTO)/lithium iron phosphate (LFP) full cell. These results demonstrate the potential for methyl carbamate to generate eutectics from lithium salts and offer alternative electrolytes for use in low-temperature Li-ion battery applications.

Introduction

Lithium-Ion (Li-ion) batteries have made it to the forefront in the quest for green energy production and electrification of vehicles to phase out fossil fuels and mitigate climate change. Since their commercialization in 1991, Li-ion batteries have dominated the field of energy storage, and most of the research has been focused on electrode materials or conventional solution-based electrolytes.[1] Specifically, carbonate-based electrolytes and their additives dominate research into the lithium-ion electrolyte.[2] While other fields of electrolytes, such as polymers, solid-state, and ionic liquids, have

been studied, deep eutectic electrolytes (DEEs) remain largely unexplored. DEEs exhibit numerous advantages over traditional electrolytes, including low cost, low-temperature operation, and low vapor pressure which leads to increased safety.[3] DEE systems are an outgrowth of research on deep eutectic solvents (DES), which are solvents that form with a mixture of two components that has a lower melting point than the individual compounds. This effect is likely caused by intermolecular interactions between the two chemicals, such as hydrogen bonding, Van der Waals, and entropy of mixing between the two components.[4] Some of the first class of DES systems were composed of quaternary ammonium salts and protic organic compounds.[5] Since then, DEEs have been developed by replacing the quaternary ammonium with metal salts, leading to a highly concentrated electrolyte as the active ion, which is an integral component of the DEE structure.[6]

DEEs recently have been applied to Li-ion batteries using lithium salts and organic components based on ureas, acetamides, sulfonamides, nitriles, and organosulfides.[3, 6-7] One common characteristic between these eutectic materials is the intermolecular interaction of Li+ to either O or N atoms in the organic compounds, which results in the deep eutectic effect.[8] Hydrogen bonding also has been shown to play a role in initiating the deep eutectic effect if both hydrogen bond donors and acceptors are present.[9] While research into lithium deep eutectics has been carried out, the field is still in its infancy and additional research can provide an unique pathway enhancement of Li-ion battery technologies. This work demonstrates the operational capability of two novel lithium DEEs based on either LiTFSI or LiPF6 mixed with methyl carbamate in a 1:5 molar ratio. Methyl carbamate represents a cheap, and high boiling point (176°C) component used to form lithium DEEs. These DEEs form spontaneously upon combining the appropriate molar ratio of precursors at room temperature with stirring as shown in Figure 1a. These novel eutectic electrolytes show excellent conductivity at room temperature and are compatible with a LTO anode and a LFP cathode, demonstrating their overall promise as alternative electrolytes for Li-ion batteries.

Results and Discussion:

Thermal gravimetric analysis (TGA) of the precursors and DEEs was measured to evaluate the temperature stability of the materials (Figure 1b). Both DEEs demonstrated greater thermal stability than pure methyl carbamate due to the strong intermolecular interactions between methyl carbamate and the lithium salt. Methyl carbamate alone showed a sublimation peak onset at ~80°C, and upon formation of the LiPF6 DEE or the LiTFSI DEE, the onset of decomposition (or sublimation) of the methyl carbamate shifted to ~115°C. This 30°C shift in

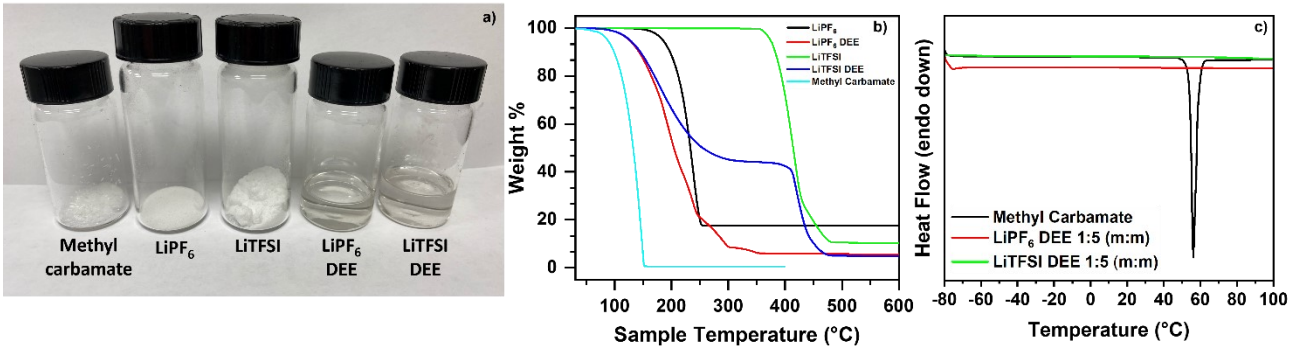

Figure 1: a) Picture of starting materials and formed DEEs. b) Thermogravimetric analysis curves of

starting materials and formed DEEs. c) Differential scanning calorimetry curves of methyl carbamate and the DEEs.

decomposition temperature indicates the formation of strong bonds that constitute the DEEs.

To confirm the synthesis of the DEEs, differential scanning calorimetry was employed to measure the melting point (Tm) (Figure 1c). The Tm of methyl carbamate was shown to be 56°C. Upon addition of LiTFSI or LiPF6 in a 1:5 molar ratio of lithium salt:methyl carbamate, a dramatic decrease in Tm was observed and resembled a glass transition (Tg) of ~-75°C, demonstrating a clear deep eutectic effect between the methyl carbamate and lithium salts. The LiTFSI DEE showed a wider range of stable ratios as compared to the LiPF6 DEE (Figure S1), likely due to the increased size of the TFSI anion leading to greater disassociation of Li+ than TFSI. LiPF6 DEEs further showed a narrower stable composition window as compared to LiTFSI DEEs. LiPF6 DEEs only spontaneously formed in a 1:6 or 1:5 m:m ratios at rt, while LiTFSI DEEs formed in 1:5 to 1:2 m:m ratios. LiPF6 DEEs also had an increased number of peaks in the DSC and while the 1:6 m:m forms at room temperature it is not stable upon cooling and heating cycle. However, stable ratios are formed only for 1:5 and 1:4 m:m whereas 1:7 to 1:6 m:m ratios have excess methyl carbamate and 1:3 – 1:1 m:m ratios have excess LiPF6. Upon heating and cooling cycle excess crystallization is seen with subsequent reforming of the mixture at higher temperatures, with the exception of LiPF6: methyl carbamate 1:1 which shows no excess peaks as it so unstable it recrystallizes at room temperature leaving a slurry of eutectic and LiPF6 crystals. LiTFSI forms stable DEEs at ratios from 1:5 to 1:2, indicating the bulkier TFSI- ion more easily disassociates. The phase diagram (Figure S2) clearly shows a wider range of stable LiTFSI DEE when compared to LiPF6. Continued investigation of the formed DEEs and their coordination properties were performed using density functional theory (DFT) and Fourier transform infrared spectroscopy (FT-IR) (Figure 2). DFT revealed a coordination between the carbonyl of methyl carbamate and the counter anion of the lithium salt in both LiPF6 and LiTFSI. This coordination led to a reduction of electron density from the carbonyl in methyl carbamate and an increase in partial positive

charge over the amine and methyl groups in methyl carbamate. Although the anionic species of the lithium salts still contained the most negative region of electrostatic potential, this charge was distributed more evenly in the presence of methyl carbamate than in LiPF6 or LiTFSI. (Figure S3).

FT-IR measurements of methyl carbamate generated absorptions at 3429 cm-1 and 3329 cm-1, which were assigned to the N-H antisymmetric and symmetric stretching vibrations, respectively. Both the LiPF6 DEE and the LiTFSI DEE showed blue shifts for these N-H stretching vibrations. Specifically, the LiPF6 DEE shifted towards 3508 cm-1 and 3410 cm-1 and the LiTFSI DEE shifted towards 3487 cm-1 and 3380 cm-1 for the antisymmetric and symmetric N-H stretching vibrations, respectively. This shift suggests a strong coordination of the Li-ion with the nitrogen atom in the methyl carbamate N-H groups.

Additionally, adsorptions at 3265 cm-1 and 3200 cm-1 were noted for methyl carbamate. These adsorptions significantly decreased for the DEE samples.

Zhao et al. has reported that these adsorptions can be attributed to methyl carbamate dimer association via hydrogen bonding, which diminishes upon cation coordination with the methyl carbamate N-H groups.[10] The bands at 1682 cm-1 and 1609 cm-1 for methyl carbamate were attributed to the C=O

stretching vibration and NH2 bending vibration, respectively. Both the LiPF6 DEE and the LiTFSI DEE showed a slight blue shift for the C=O stretching vibration and a slight red shift for the N-H bending vibration. Specifically, LiPF6 DEE shifted to 1690 cm-1 and 1597 cm-1 and the LiTSFI DEE shifted to 1691 cm-1 and 1598 cm-1 for the C=O stretching vibration and N-H bending vibration, respectively. Taken together, the data suggest that the Li-ions for each electrolyte are coordinating with the nitrogen atoms of the N-H groups of the methyl carbamate, causing blue shifts for the antisymmetric and symmetric N-H stretching vibrations and the C=O stretching vibration and a red shift for the N-H bending vibration.

Electrochemical impedance spectroscopy (EIS) was performed to evaluate the conductivity of the resulting DEEs. Specifically, EIS was employed to determine which fully soluble DEE ratio (1:2 to 1:5, mol:mol) (Figure S4) had the optimal ionic conductivity to facilitate battery performance (Figure S5). LiTFSI-based DEEs showed the highest conductivity (at room temperature) for a 1:5 molar ratio, decreasing as the lithium salt concentration in LiTFSI:methyl carbamate was increased to a ratio of 1:2. LiPF6 DEEs showed a similar trend with a maximum conductance observed with the 1:5 LiPF6:methyl carbamate ratio, decreasing conductivity with increasing concentration of LiPF6 salt. This phenomenon is most likely due to a decrease in the coordination between the lithium cation and the corresponding anion upon additional coordination with methyl carbamate and a decreased viscosity in higher molar ratios of methyl carbamate as seen in previous DEE systems. This decrease in the anion and cation interaction strengths and this decrease in viscosity facilitate Li-ion transport across the electrolyte. [7c] To support this claim, conductivity and viscosity measurements were performed to study the temperature dependence of the conductivity (Figure 3). A strong correlation between ionic conductivity (σ) and temperature (T) was observed. At 0°C the conductivity was 7.78E-4 and 8.26E-4 S•cm-1 for LiPF6 DEE and LiTFSI DEE, respectively (Figure 3a). Upon heating the LiPF6 and LiTFSI DEEs, conductivity increased to 3.16E-3 S•cm-1 and 2.87E-3 S•cm-1 at

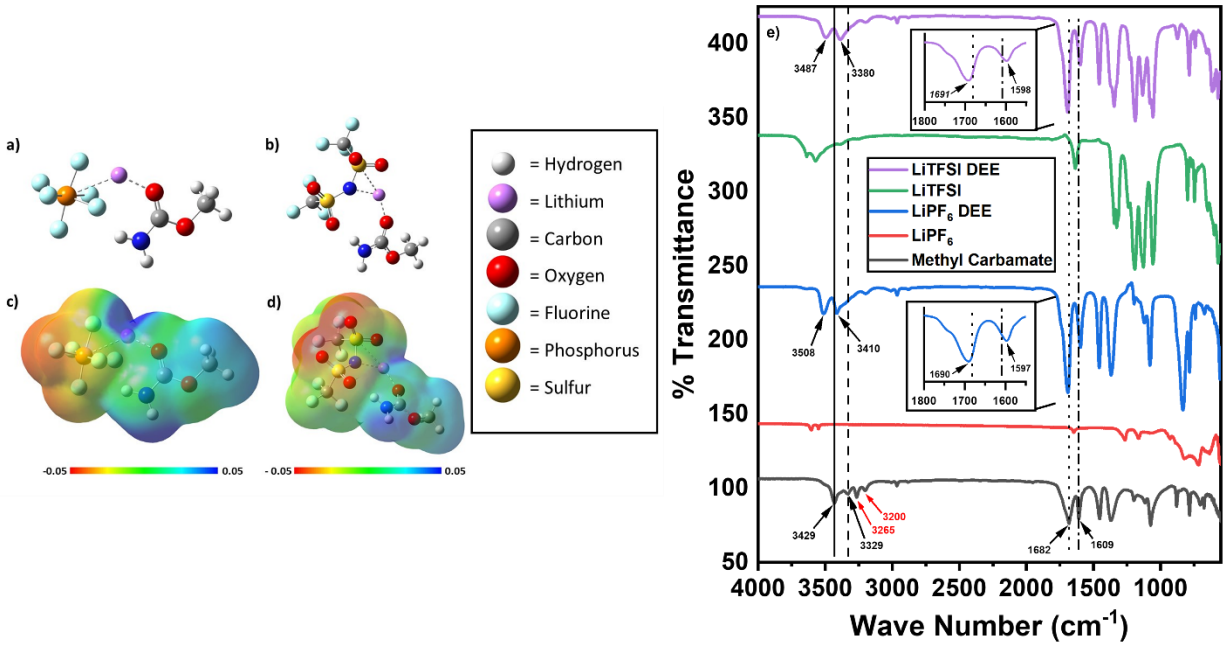

Figure 2: a) Coordination environment between LiPF6 and methyl carbamate, b) coordination environment between LiTFSI and methyl carbamate, c) molecular electrostatic potential map of LiPF6:methyl carbamate, and d) molecular electrostatic potential map of LiTFSI: methyl carbamate. e) IR of DEEs and starting materials.

25°C and 1.38E-2 S•cm-1 and 1.0E-2 S•cm-1 at 80°C, respectively. Viscosity measurements showed a decrease in viscosity with an increase in temperature, demonstrating a clear correlation between lower viscosity and higher conductance as would be expected (Figure 3b). Interestingly, the DEEs did not show a linear Arrhenius-like log(σ) vs. temperature (1000/T) behavior but did demonstrate a linear Vogel-Tammann-Fulcher (VTF) dependance of log(σ) vs (log1000/(T-T0) (T0 is glass transition temperature seen in DSC) (Figure S6). VTF linearity coupled with the strong correlation of viscosity and conductivity suggests the main ionic mobility parameters and charge transport correlate to the methyl carbamate's molecular motion in the DEEs.

Cyclic voltammetry (CV) was utilized to characterize the electrochemical stability windows of the DEEs (Figure 3c). CVs on LiTFSI showed a stability window of ~1.6 V to ~5 V vs (Li/Li+), indicating high voltage stability and allowing for cathodes such as LFP to be utilized; however, LiPF6 DEEs showed an ever-wider stability window of ~1 V to ~5 V vs (Li/Li+). Such a stability window suggests that the DEEs should be able to accommodate a LTO/LFP full cell. However, methyl carbamate DEEs do not seem to form a stable solid electrolyte interphase (SEI) without additives, as Li/Li symmetric cycling showed rapid voltage overpotential degradation (Figures S7). However, electrochemical stability may be imparted in future studies by adding SEI forming additives such as lithium nitrate or ethylene carbonate. The demonstration of the methyl carbamate based DEEs as electrolytes in LTO/LFP full cells was performed using galvanostatic cycling experiments in coin cells using 2.05V to .5V charge/discharge cutoffs. The stability and voltage profiles for the LiPF6 DEE containing full cells showed good cycling stability at moderate charge/discharge rates (0.5C) with an initial conditioning cycle "0" followed by 50 additional cycles (Figure 4).

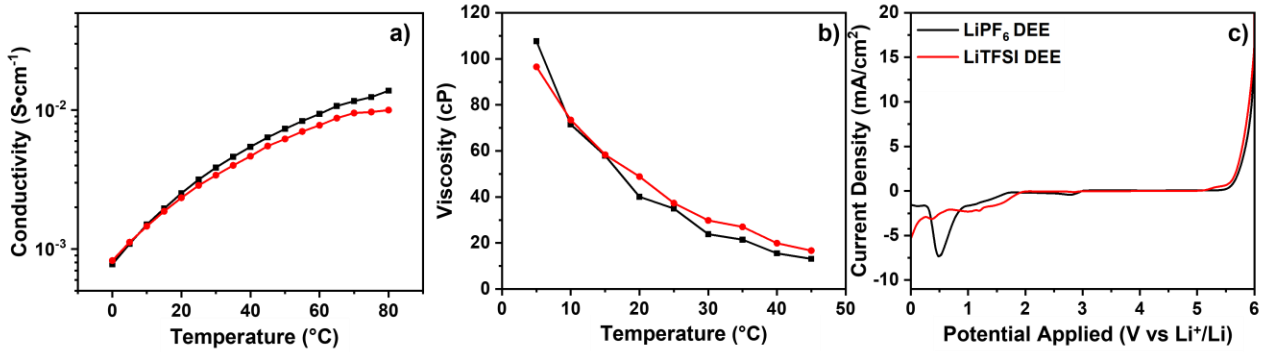

Figure 3: a) Ionic conductivity of DEEs at different temperatures. b) Viscosity of DEEs as a function of temperature. c) Cyclic voltammetry of DEEs at 25 mV/s sweep rate with Pt|Li|Li three electrode setup.

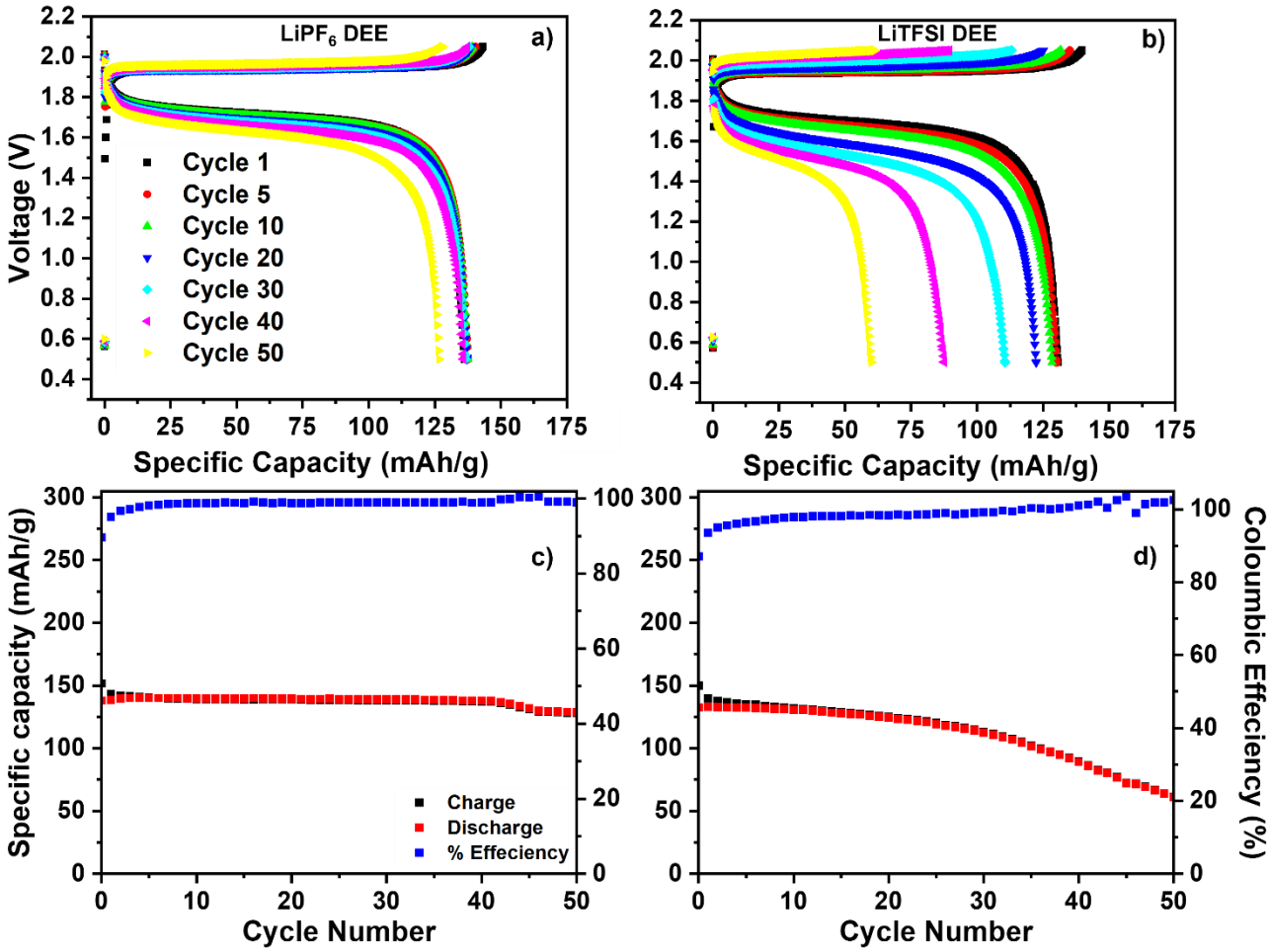

Figure 4: a-b) Voltage profiles of (a) LiPF6 DEE and (b) LiTFSI DEE, c-d) Cycling performance and efficiency of (c) LiPF6 DEE and (d) LiTFSI DEE

An initial 5.5% charging capacity loss and a 0.3% increase in discharge capacity were seen after the initial conditioning cycle with 84% efficiency and a discharge capacity of 136 mAh•g-1 for LiPF6 DEE full cells. Roughly a 99% efficiency after the initial conditioning cycle charging was observed with a charging capacity retention of 95.9% from cycle 1 to 40, with a further 99.7% percent discharge capacity retention. However, between cycle 1 and cycle 50, a charge and discharge capacity loss of 89.4% and 93.0% were seen, showing good initial cycling characteristics.

The LiTFSI-based DEE showed a ~130 mAh•g-1 initial discharge capacity with a 6.7% initial loss of charge capacity and 0.3% discharge capacity gain after the conditioning cycle. Starkly, after 50 cycles only a 43.8% charge capacity and 45.9% discharge capacity were retained. We attributed this loss to the LiTFSI DEE having a ~0.6V higher reduction potential as opposed to the LiPF6 DEE, which is more electrochemically unstable, leading to more significant capacity losses. To study the cycling rate dependance on cell capacity, further cycling of the DEEs was performed at different rates (0.25C, 0.5C, and 1C), with the 0.5C rate was performed at an elevated temperature of 50°C (Figure S8-10). At 0.25C

cycling rates, high first cycle discharge capacities of 172 mAh•g-1 (LiPF6 DEE) and 175 mAh•g-1 (LiTFSI DEE) were observed. However, a much smaller percent capacity retention of 72% and 78% for the LiPF6 and LiTFSI DEEs, respectively, were noted. These efficiencies were lower when compared to the 0.5C rates. Interestingly, at lower charge rates LiTFSI DEEs performed better and had a higher discharge capacity retention rate than the LiPF6 DEEs. However, when high charge rates and high temperatures were used, LiPF6 DEEs had far superior capacity retention and efficiencies, especially at elevated temperatures (50°C), in which the LiTFSI DEE full cells failed after 10 cycles. When the 1C rate was used, a much lower capacity retention was observed, especially with the LiTFSI DEE containing system.

The initial interfacial resistance decreased dramatically after cycling (Figure S11). A clear trend of faster cycling leading to smaller interfacial resistances and decreasing cycling rates leading to larger resistance was observed. While Li/Li symmetric cell cycling showed no stable SEI formation, the fast cycling of the full cell may have allowed for less reductive decomposition time. This SEI formation was observed, as two higher resistance semicircles appeared at low cycle rates for LiPF6 DEEs as compared to the one seen in LiTFSI DEEs at low cycle rates. Furthermore, at 50°C a substantial increase in resistance was observed, showing the instability of these DEEs at elevated temperatures. One advantage for DEEs is the possibility of low-temperature cell operation indicated by powering an LED at 45 °C (Figure S12).

Scanning electron microscopy (SEM) showed little to no change in particle morphology for the LTO or the LFP electrodes even with higher temperature cycling (Figures S13-15), suggesting that LTO and LFP have good compatibility with the methyl carbamate-based DEE.

Conclusion:

In conclusion, we have shown the development and application of a new DEE incorporating LiPF6 or LiTFSI with methyl carbamate. The primary DEEs were formed by coordination of Li-ions with the carbonyl of methyl carbamate and a delocalization of electron density over the complex due to strong electrostatic interactions. At molar ratios of 1:5 (salt:methyl carbamate), we have demonstrated promising initial electrochemical characteristics of the DEEs with a large electrochemical stability window of 1V to 5V versus Li/Li+ and good ionic conductivity of 3.16E-3 S•cm-1 at 25°C. We have further demonstrated the compatibility of these DEEs with LTO and LFP in full cells. A reversible capacity of 128 mAh•g-1 after 50 cycles and a 93% discharge capacity retention were observed. This system was even shown to be operational at substantially reduced temperatures with the capability of powering a LED at -45°C. The characterization of this system provides further insight into the potential of DEEs as alternative electrolytes for Li-ion batteries and demonstrates the potential for methyl carbamate to generate eutectics from lithium salts.

Experimental:

Materials: Lithium bis(trifluoromethanesulfonyl)amide (LiTFSI) and lithium hexaflourophosphate were purchased from TCI chemicals. Methyl carbamate was purchased from Thermo Fisher and was double recrystallized from hot anhydrous benzene and dried under vaccum before use. Premade LiFePO4 (LFP) cathode foils, lithium titanate (LTO) powders, and CR2025 coin cells were purchased from MTI. Acetylene black, polyvinylidene difluoride (PVDF), lithium metal, anhydrous benzene, and n-methyl pyrrolidone (NMP) were purchased from Sigma Aldrich.

LTO cathodes were cast using a slurry NMP solvent with mass fractions of 85% LTO, 10% acetylene black, and 5% PVDF binder. The obtained cathode slurry was coated on Al foil in air and dried in a vacuum oven at 120 ºC overnight. Foils were cut into 16 mm diameter circles. All other synthesis and fabrication were done in an argon glovebox or under argon on a Schlenk line. LFP was dried overnight at 100°C under vacuum.

Deep eutectic electrolyte (DEE) synthesis: DEEs with a 1:5 m:m were synthesized by mixing the lithium salt with methyl carbamate at room temperature (RT). For other ratios (1:7 – 1:1) the DEEs were stirred for 2 hours at 70°C if they did not form without heat.

FT-IR: Fourier transform infrared spectroscopy measurements were carried out on a Jasco 4200 using an attenuated total reflectance (ATR) attachment equipped with a ZnSe prism under nitrogen purge. Sixty-four scans with a resolution of 2 cm-1 were collected in the region of 4000-550 cm-1 for each spectrum. Samples were held under argon until briefly being exposed to the atmosphere for sample loading.

DFT: Density functional theory calculations were carried out using the Gaussian 16 platform.[11] Molecular structures were first geometry optimized using the M06-2X functional paired with the triple zeta Pople basis set 6-311g with polarization and diffuse functions on all atoms. Molecular electrostatic potential maps were generated in the GaussView6 program.[12]

Electrochemical analysis: A BioLogic multichannel potentiostat was used for all electrochemical experiments. CR2025 coin cells were used for cell cycling. LFP|LTO full cells were fabricated by adding LFP electrode then glass fiber separator soaked in DEE electrolyte then LTO electode. Li|Li symmetric cells were fabricating using the same process. LFP|LTO full cells were cycled from 2.05V to 0.5V. Galvanostatic Li|Li cycling was done using a current of 0.50 mA with 10 minute charge discharge cycles. LSV was performed using a 10 mv/s scan rate with a lower limit of 0 V to 6 V vs Li0/Li+. Electrochemical Impedance Spectroscopy (EIS) was measured before and after cycling from 1 MHz to 1 Hz. For low temperature LED operation, 2 coin cells were used in series and submerged in an acetonitrile slurry chilled with liquid nitrogen and then attached to a blue LED using alligator clips.

Ionic conductivity measurements: The Ionic conductivities were measured using DEEs using a coin cell setup with 2 stainless steel foil electrodes and a rubber washer as the separator with an inner diameter of .45cm and a thickness of .144 cm to .115 cm (gaskets were measured for thickness using a caliper before and after coin cell crimping). After dripping the DEEs into the middle and crimping the cell, EIS was measured from 200 kHz to 100 mHz and from temperatures 0 °C to 80 °C. The ionic conductivity was calculated using $\sigma = L/ (Z \times A)$, where Z is the impedance for the real axis, A is the area of the gasket hole, and L is the thickness of the gasket.

Differential scanning calorimetry: DSC measurements were performed using a TA Q20 with a RSC90 chiller with a rate of 5 °C/min from -90 °C to 100 °C.

Scanning electron microscopy: SEM measurements on LTO and LFP electrodes were done before and after cycling using a Hitachi 8230. After cycling coin cells were de-crimped and electrodes were washed with ether before being dried. Images were taken at 10K and 50K magnification.

Acknowledgements:

This work was supported by the Laboratory Directed Research and Development (LDRD) program within the Savannah River National Laboratory (SRNL). This work was produced by Battelle Savannah River Alliance, LLC under Contract No. 89303321CEM000080 with the U.S. Department of Energy.

Publisher acknowledges the U.S. Government license to provide public access under the DOE Public Access Plan (https://www.energy.gov/downloads/doe-public-access-plan).

Keywords: deep eutectic electrolyte · energy conversion · energy storage · lithium-ion battery · low temperature battery

Entry for the Table of Contents

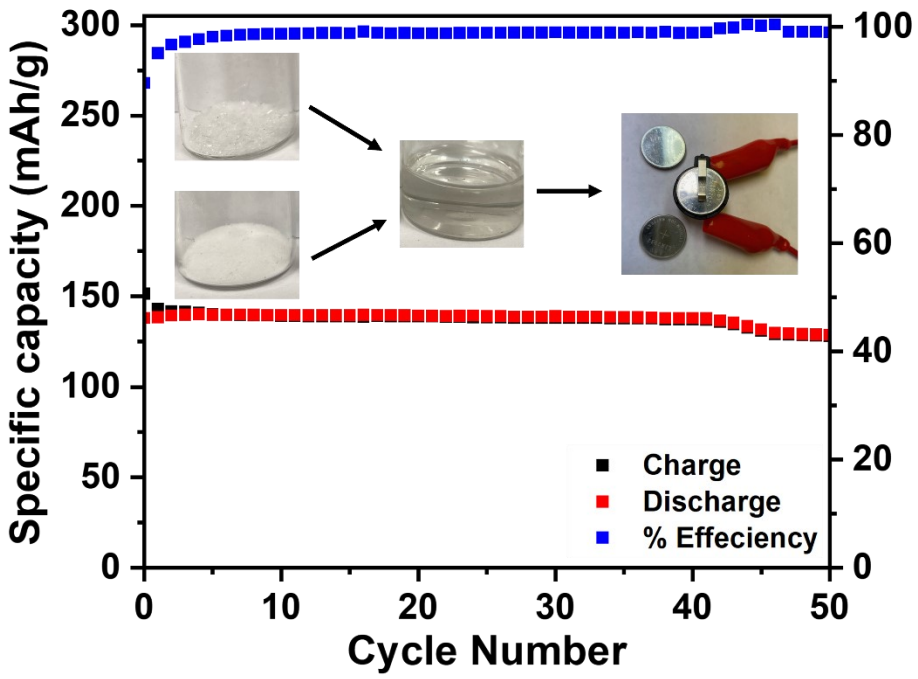

A novel binary deep eutectic electrolyte was developed using lithium salts and methyl carbamate. The deep electrolyte showed promising electrochemical behavior in a lithium titanate and lithium iron phosphate full cell, allowing for stable cycling and low temperature operation.

References:

[1] a) R. Marom, S. F. Amalraj, N. Leifer, D. Jacob, D. Aurbach, Journal of Materials Chemistry 2011, 21, 9938-9954; b) W. Lee, S. Muhammad, C. Sergey, H. Lee, J. Yoon, Y.-M. Kang, W.-S. Yoon, Angewandte Chemie International Edition 2020, 59, 2578-2605; c) A. Kraytsberg, Y. Ein-Eli, Advanced Energy Materials 2012, 2, 922-939; d) K. Li, Z. Hu, J. Ma, S. Chen, D. Mu, J. Zhang, Advanced Materials 2019, 31, 1902399; e) S. S. Zhang, Journal of Power Sources 2006, 162, 1379-1394.

[2] a) D. Aurbach, Y. Talyosef, B. Markovsky, E. Markevich, E. Zinigrad, L. Asraf, J. S. Gnanaraj, H.-J. Kim, Electrochimica Acta 2004, 50, 247-254; b) L. Chen, K. Wang, X. Xie, J. Xie, Journal of Power Sources 2007, 174, 538-543; c) A. Wang, S. Kadam, H. Li, S. Shi, Y. Qi, npj Computational Materials 2018, 4, 15.

[3] H. Ogawa, H. Mori, Physical Chemistry Chemical Physics 2020, 22, 8853-8863.

[4] a) A. Shishov, A. Bulatov, M. Locatelli, S. Carradori, V. Andruch, Microchemical Journal 2017, 135, 33-38; b) B. B. Hansen, S. Spittle, B. Chen, D. Poe, Y. Zhang, J. M. Klein, A. Horton, L. Adhikari, T. Zelovich, B. W. Doherty, B. Gurkan, E. J. Maginn, A. Ragauskas, M. Dadmun, T. A. Zawodzinski, G. A. Baker, M. E. Tuckerman, R. F. Savinell, J. R. Sangoro, Chemical Reviews 2021, 121, 1232-1285.

[5] A. P. Abbott, D. Boothby, G. Capper, D. L. Davies, R. K. Rasheed, Journal of the American Chemical Society 2004, 126, 9142-9147.

[6] a) Z. Hu, F. Xian, Z. Guo, C. Lu, X. Du, X. Cheng, S. Zhang, S. Dong, G. Cui, L. Chen, Chemistry of Materials 2020, 32, 3405-3413.

b) A. Fukunaga, T. Nohira, Y. Kozawa, R. Hagiwara, S. Sakai, K. Nitta, S. Inazawa, Journal of Power Sources 2012, 209, 52-56.

c) Y. Ding, C. Zhang, L. Zhang, H. Wei, Y. Li, G. Yu, ACS Energy Letters, 2018, 3, 2641-2648. d) C. Zhang, Y. Ding, L. Zhang, X. Wang, Y. Zhao, X. Zhang, G. Yu, Angewandte Chemie International Edition 2017, 56, 7454-7459.

[7] a) V. Lesch, A. Heuer, B. R. Rad, M. Winter, J. Smiatek, Physical Chemistry Chemical Physics 2016, 18, 28403-28408; b) O. E. Geiculescu, D. D. DesMarteau, S. E. Creager, O. Haik, D. Hirshberg, Y. Shilina, E. Zinigrad, M. D. Levi, D. Aurbach, I. C. Halalay, Journal of Power Sources 2016, 307, 519-525; c) J. Song, Y. Si, W. Guo, D. Wang, Y. Fu, Angewandte Chemie International Edition 2021, 60, 9881-9885; d) A. Boisset, S. Menne, J. Jacquemin, A. Balducci, M. Anouti, Physical Chemistry Chemical Physics 2013, 15, 20054-20063.

[8] H. Ogawa, Y. Sato, H. Mori, Materials Chemistry Frontiers 2021, 5, 8078-8085.

[9] a) D. Yu, Z. Xue, T. Mu, Chemical Society Reviews 2021, 50, 8596-8638; b) E. L. Smith, A. P. Abbott, K. S. Ryder, Chemical Reviews 2014, 114, 11060-11082.

[10] W. Zhao, F. Wang, W. Peng, N. Zhao, J. Li, F. Xiao, W. Wei, Y. Sun, Industrial & Engineering Chemistry Research 2008, 47, 5913-5917.

[11] M. J. Frisch, G. W. Trucks, H. B. Schlegel, G. E. Scuseria, M. A. Robb, J. R. Cheeseman, G. Scalmani, V. Barone, G. A. Petersson, H. Nakatsuji, X. Li, M. Caricato, A. V. Marenich, J. Bloino, B. G. Janesko, R. Gomperts, B. Mennucci, H. P. Hratchian, J. V. Ortiz, A. F. Izmaylov, J. L. Sonnenberg, F. Williams, F. Ding, F. Lipparini, F. Egidi, J. Goings, B. Peng, A. Petrone, T. Henderson, D. Ranasinghe, V. G. Zakrzewski, J. Gao, N. Rega, G. Zheng, W. Liang, M. Hada, M. Ehara, K. Toyota, R. Fukuda, J. Hasegawa, M. Ishida, T. Nakajima, Y. Honda, O. Kitao, H. Nakai, T. Vreven, K. Throssell, J. A. Montgomery Jr., J. E. Peralta, F. Ogliaro, M. J. Bearpark, J. J. Heyd, E. N. Brothers, K. N. Kudin, N. N. Staroverov, T. A. Keith, R. Kobayashi, J. Normand, K. Raghavachari, A. P. Rendell, J. C. Burant, S. S. Iyengar, J. Tomasi, M. Cossi, J. M. Millam, M. Klene, C. Adamo, R. Cammi, J. W. Ochterski, R. L. Martin, K. Morokuma, O. Farkas, J. B. Foresman, D. J. Fox, *Gaussian 16 Rev. C.01*, Wallingford, CT,

[12] Dennington, R.; Keith, T. A.; Millam, J. M. GaussView, Version 6, 2016, Semichem Inc., Shawnee Mission, KS, 2016.

Supporting Information

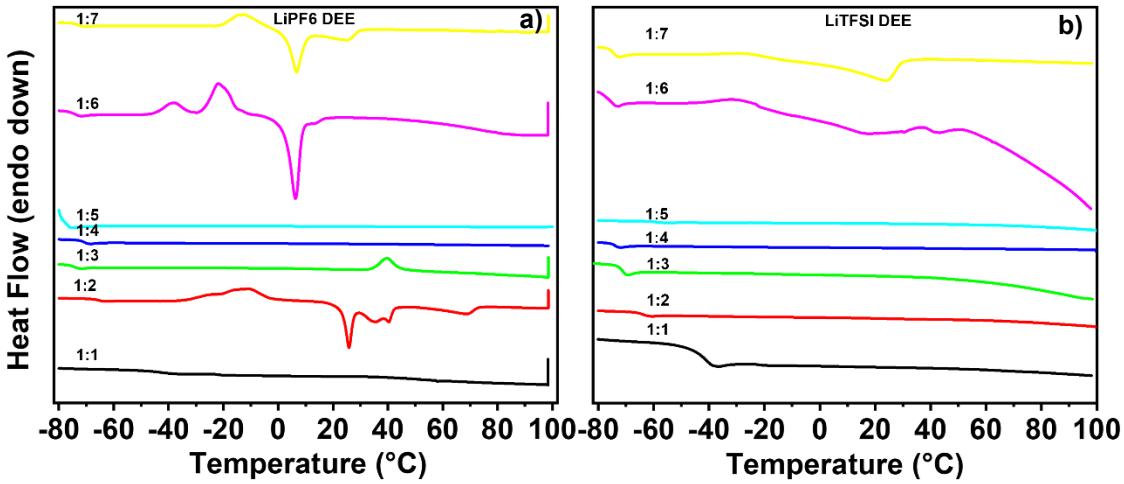

Figure S1: DSC of various a) $LiPF_6$ and b) LiTFSI DEE with salt:methyl carbamate m:m ratios.

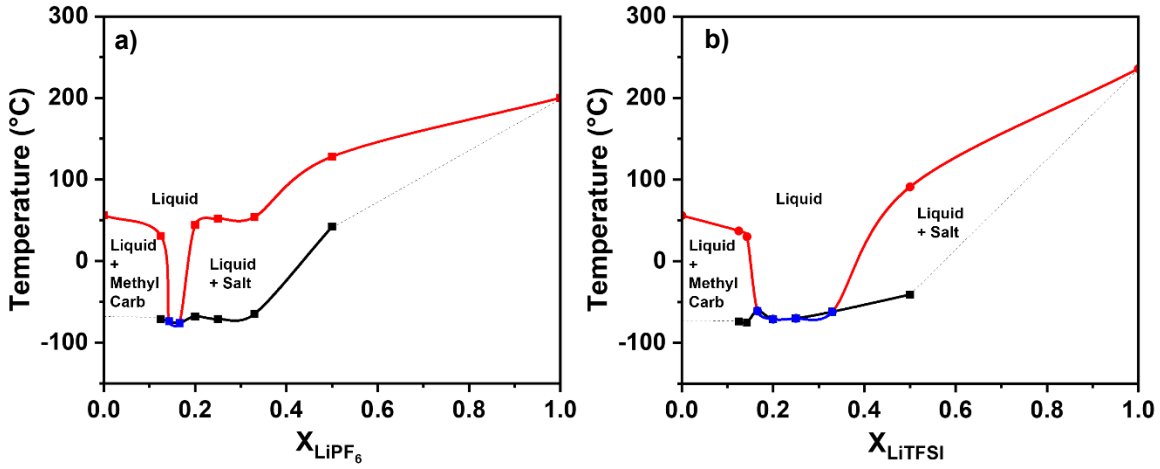

Figure S2: Phase diagrams of a) $LiPF_6$:methyl carbamate and b) LiTFSI:methyl carbamate. Red points represent melting temperature required to initially form DEE (if not spontaneous at room temperature) and MP of starting materials, black points are T_g of lowest phase transition of DEE. Blue points are to show deep eutectic region where eutectic formation is spontaneous with no noticble DSC signals above the T_g.

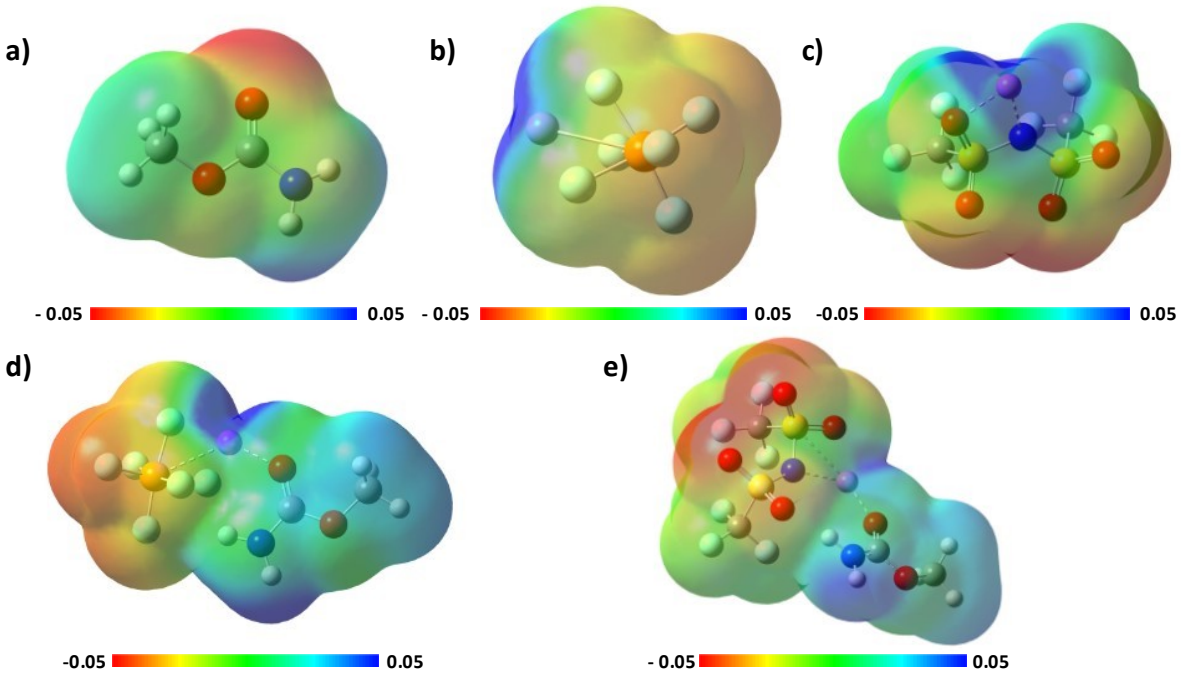

Figure S3 a) molecular electrostatic density maps of a) methyl carbamate b) $LiPF_6$ c) LiTFSI d) $LiPF_6$-Methyl Carbamate e) LiTFSI-Methyl Carbamate

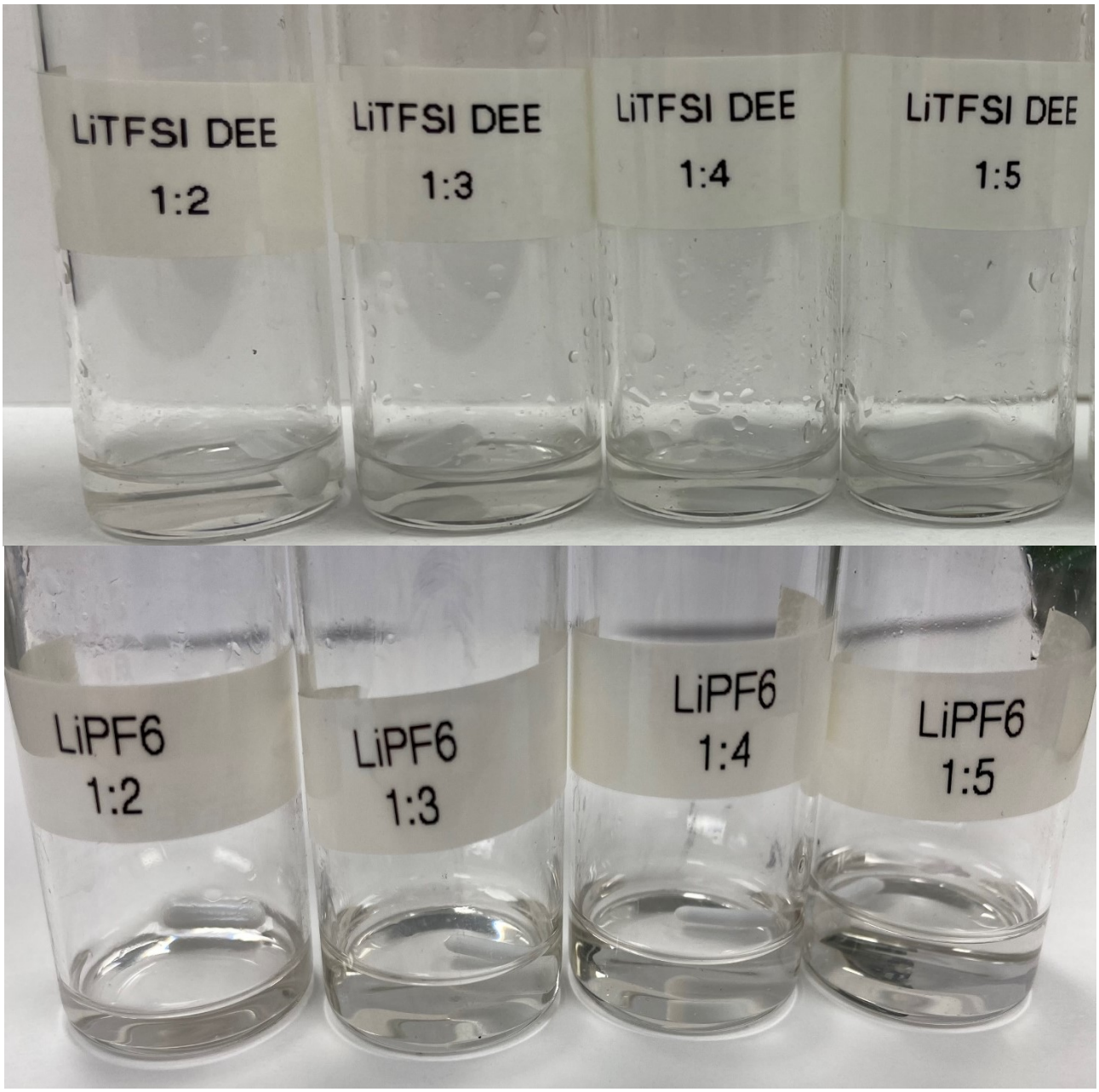

Figure S4: Formation DEEs at different ratios for LiTFSI (top) and $LiPF_6$ (Bottom)

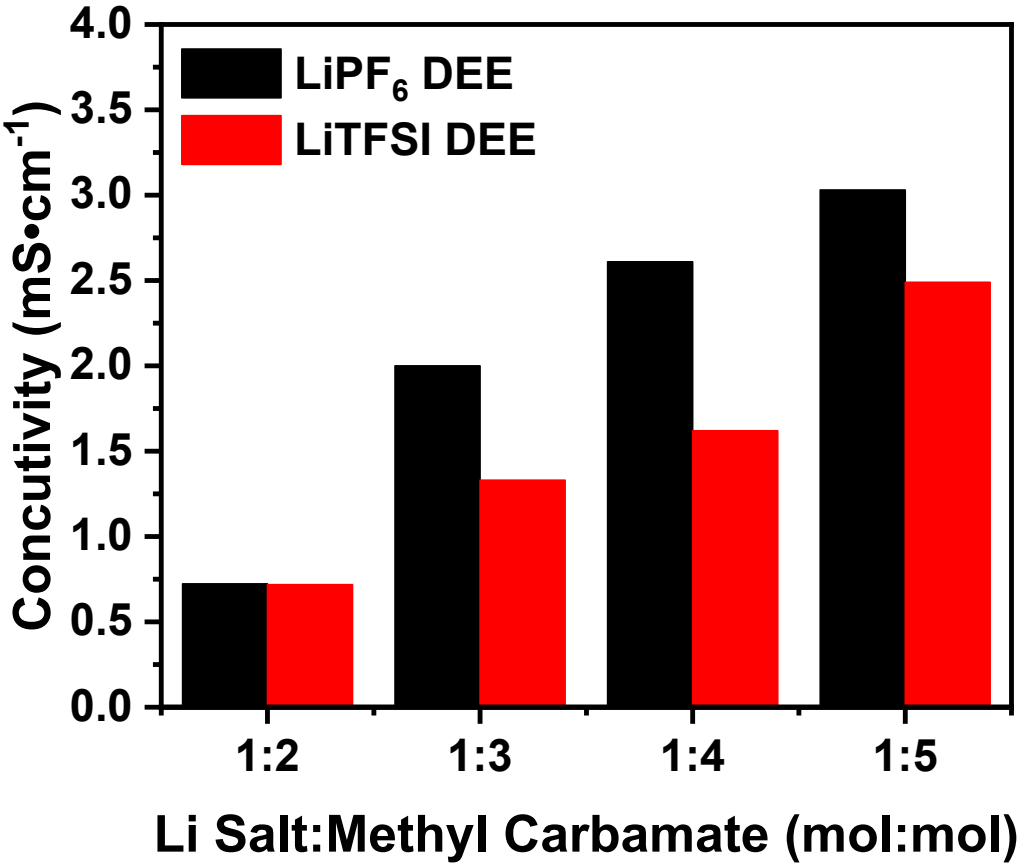

Figure S5: Conductivity of Li DEEs at different Li salt:methyl carbamate ratios.

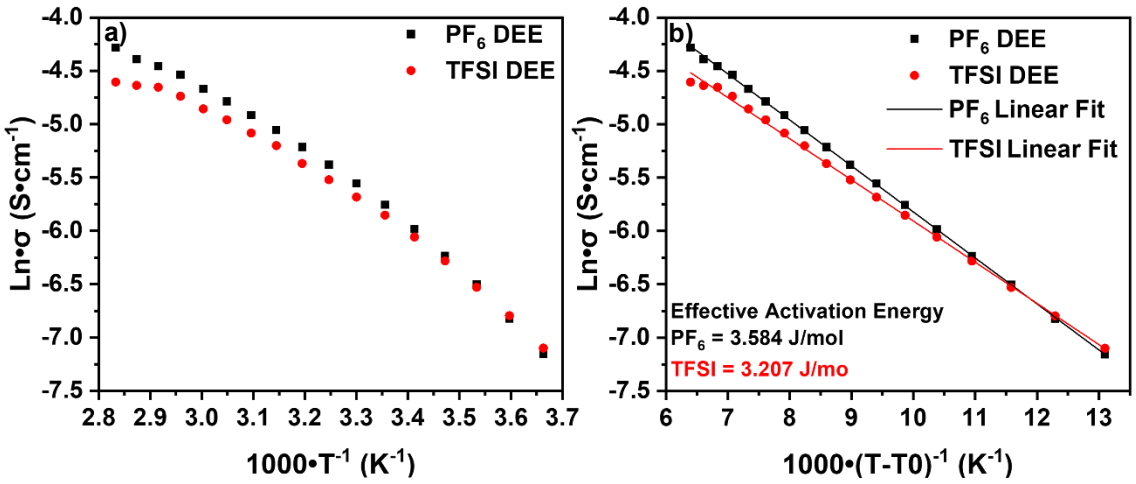

Figure S6: a) Arrhenius and b) VTF plots of Li DEEs showing the relationship of conductivity and temperature.

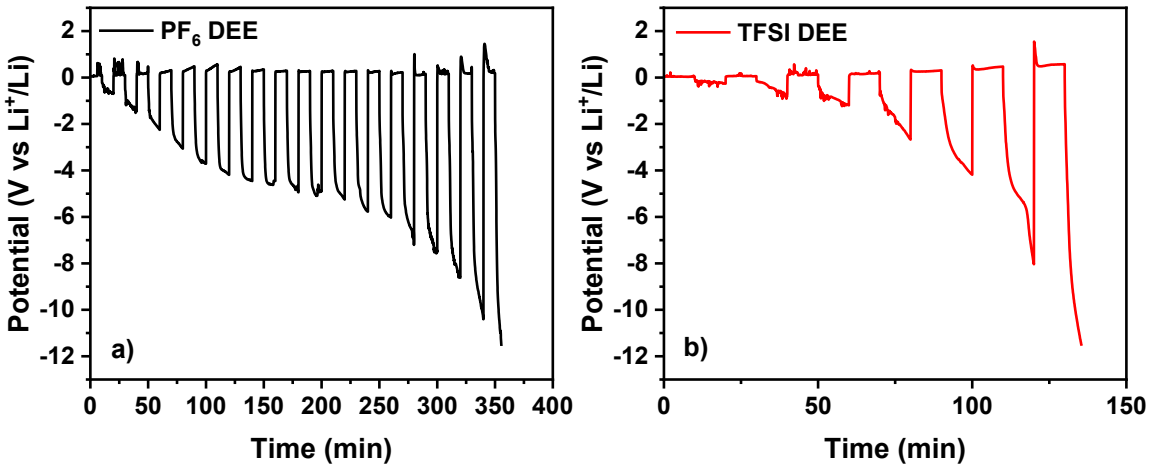

Figure S7: Symmetric galvanostatic cycling of Li|Li coin cells using a) $LiPF_6$ and b) LiTFSI DEEs at a current of 0.50 mA.

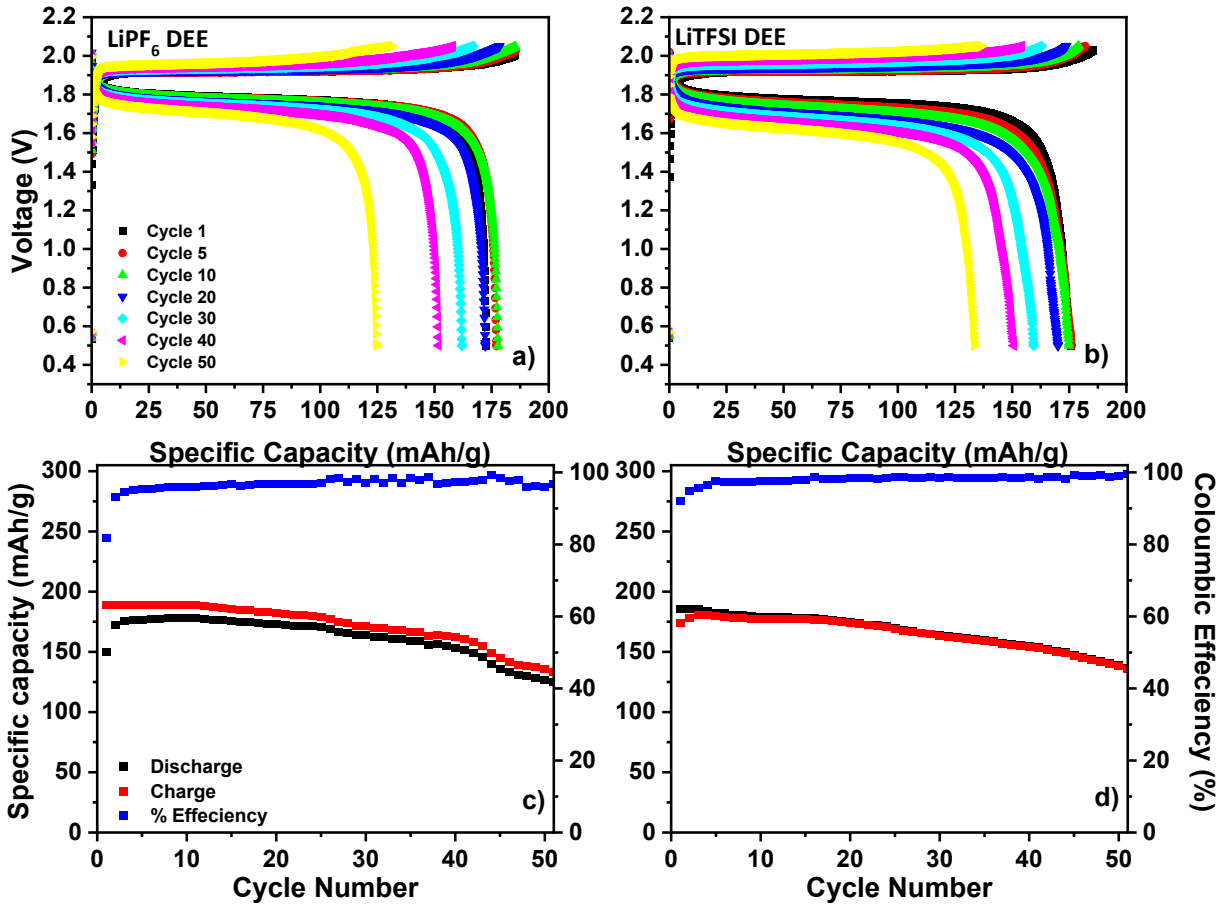

Figure S8: Voltage profiles of LTO|LFP at 0.25 C rate for a) $LiPF_6$ DEE and b) LiTFSI DEE. Cycling performance of full cells for c) $LiPF_6$ DEE and d) LiTFSI DEE at 0.25 C rate.

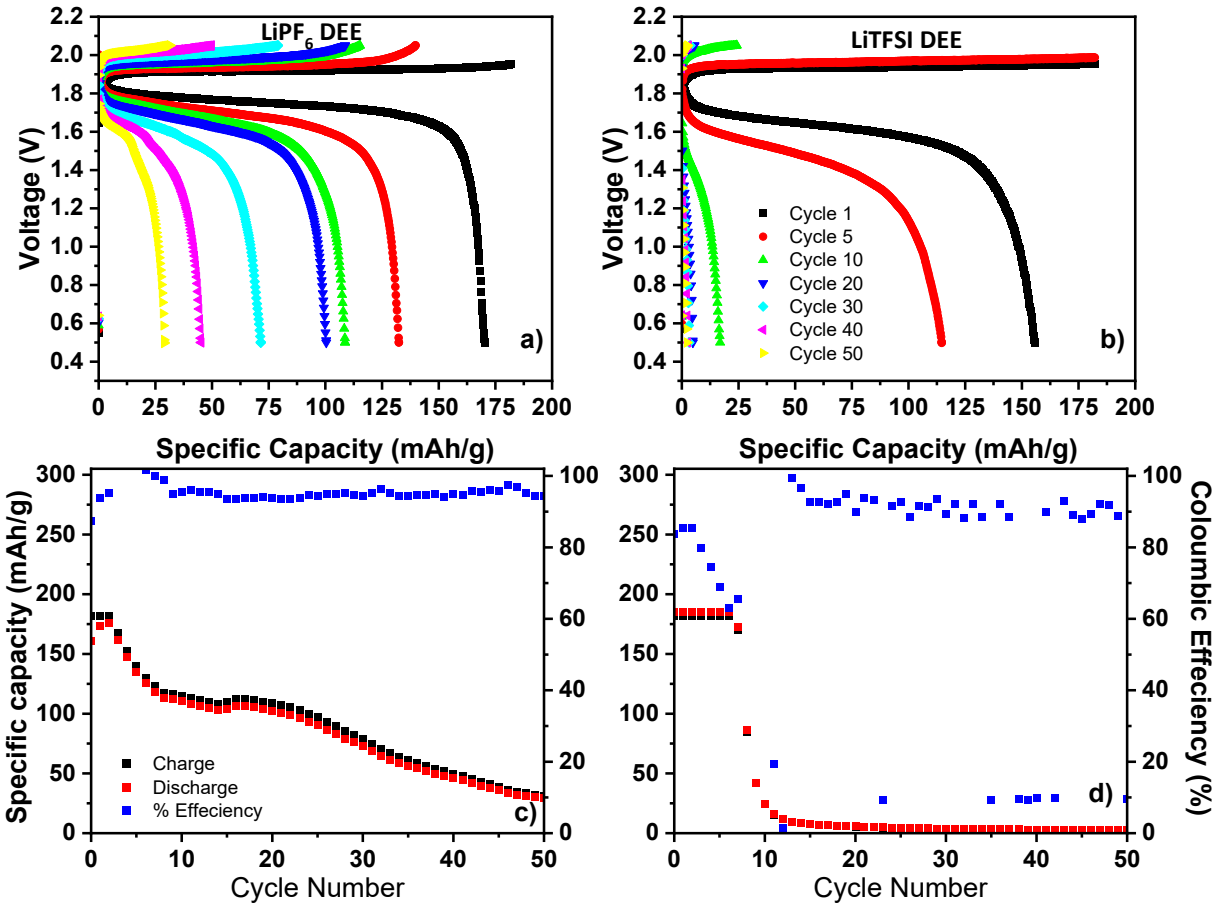

Figure S9: Voltage profiles of LTO|LFP at 0.5 C rate and 50 °C for a) $LiPF_6$ DEE and b) LiTFSI DEE. Cycling performance of full cells for c) $LiPF_6$ DEE and d) LiTFSI DEE at 0.50 C rate and 50 °C.

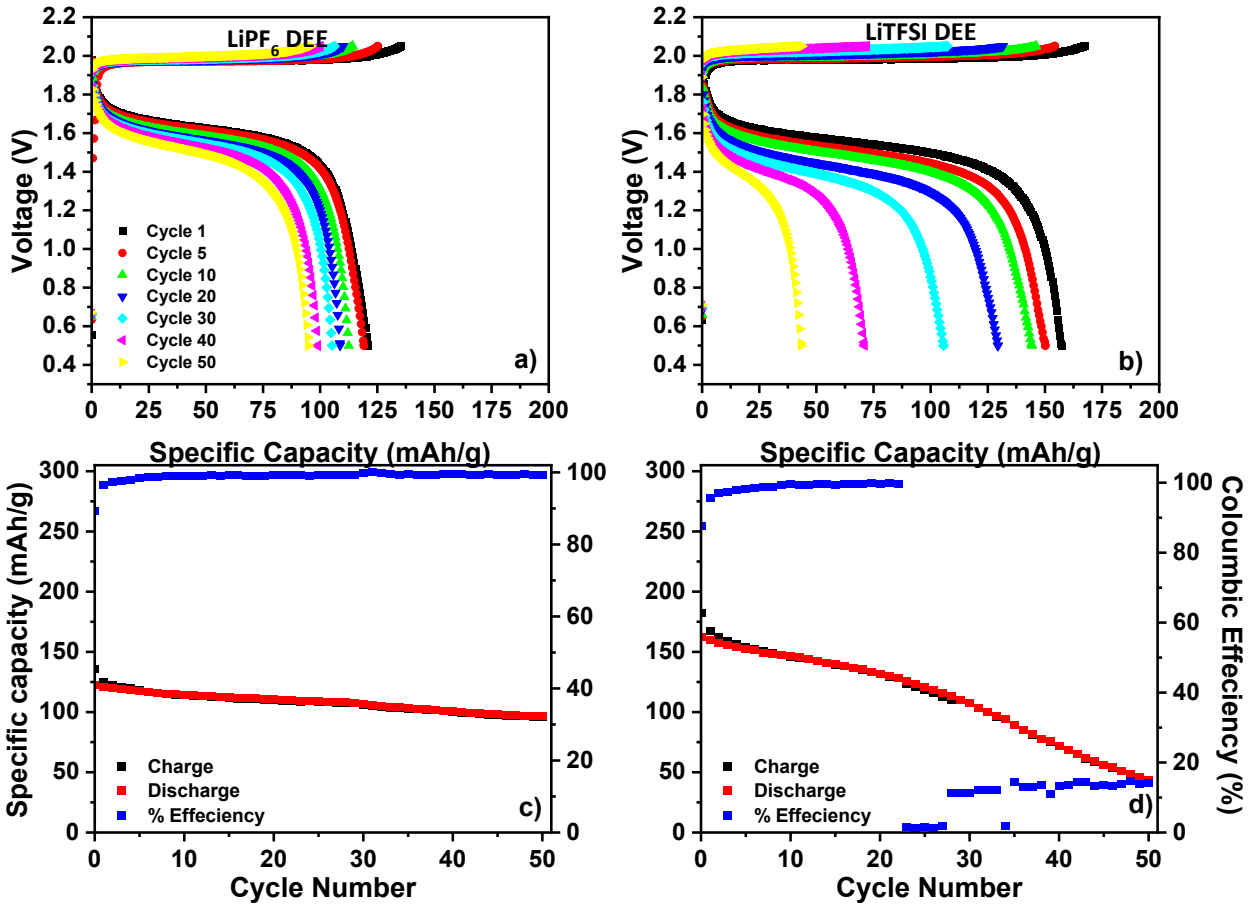

Figure S10: Voltage profiles of LTO|LFP at 1 C rate for a) $LiPF_6$ DEE and b) LiTFSI DEE. Cycling performance of full cells for c) $LiPF_6$ DEE and b) LiTFSI DEE at 1 C rate.

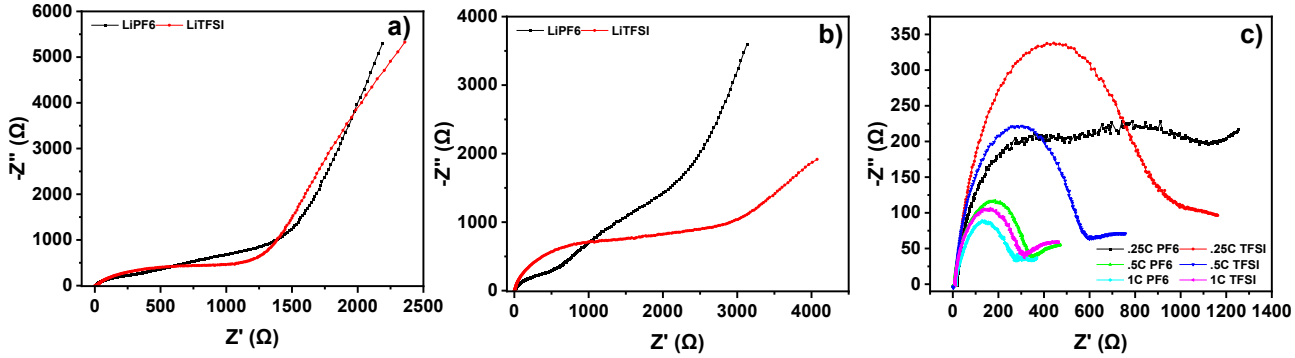

Figure S11: Nyquist plots of LTO|LFP full cells. a) EIS before cycling, b) EIS after cycling at 50 °C, and c) EIS after cycling at different rates.

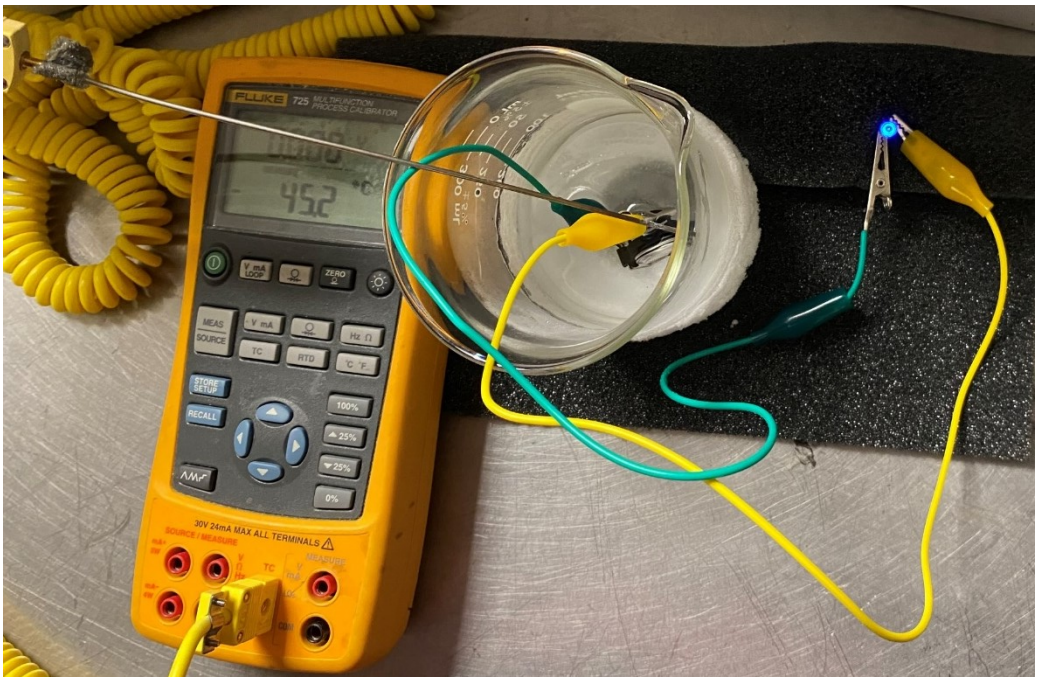

Figure S12: Low temperature operation of LTO|$LiPF_6$ DEE|LFP full cell powering a blue LED.

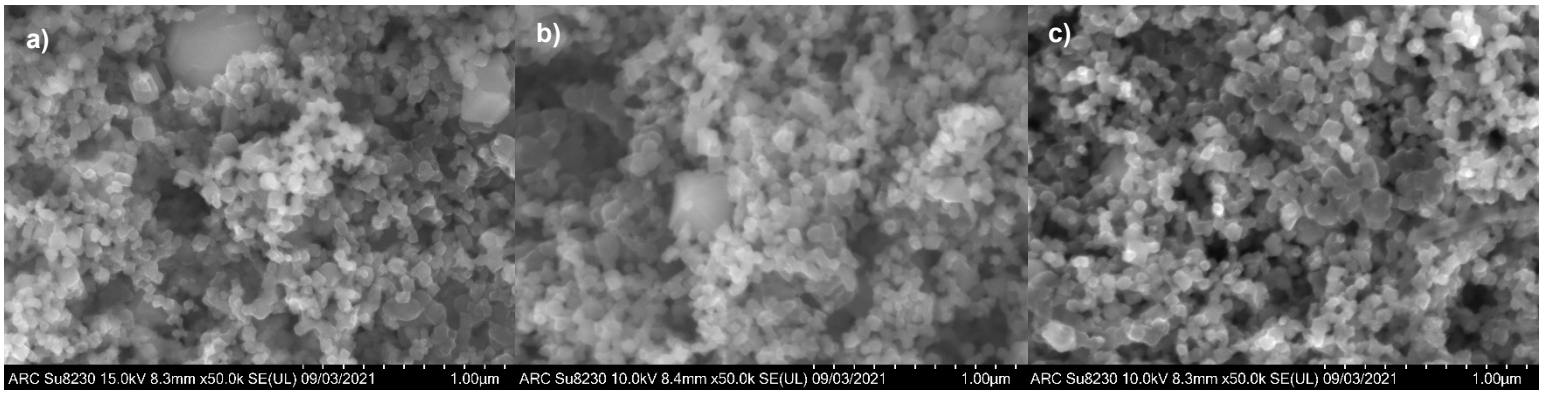

Figure S13: SEM images of Pristine a) LTO, b) LTO anode after 50 cycles at 0.5 C, and c) 0.5 at 50 °C using $LiPF_6$ DEE.

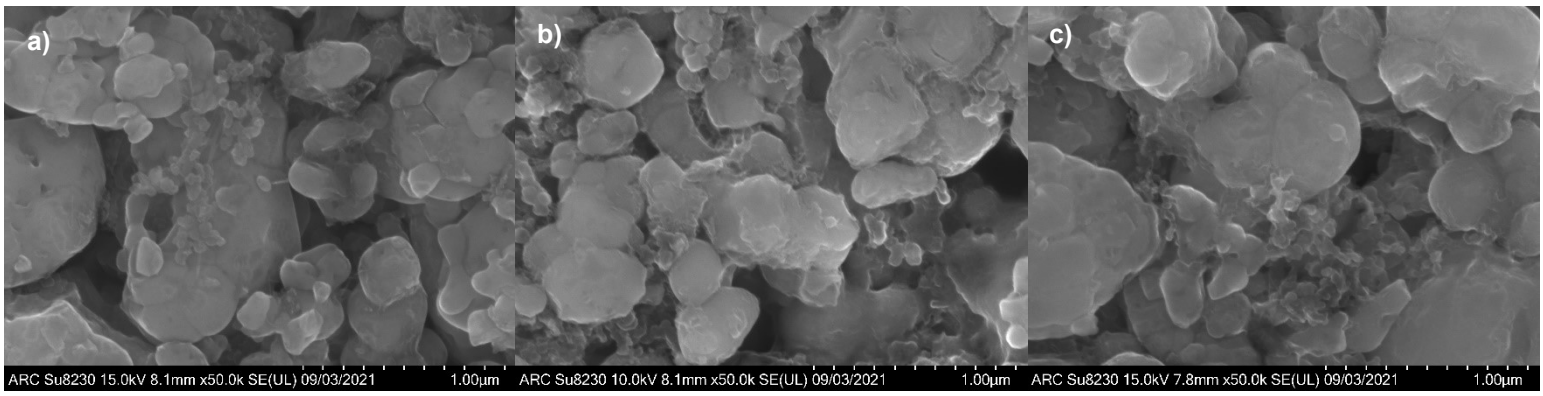

Figure S14: SEM images of a) Pristine LFP, b) LFP anode after 50 cycles at 0.5 C, and c) 0.5 at 50 °C using $LiPF_6$ DEE.

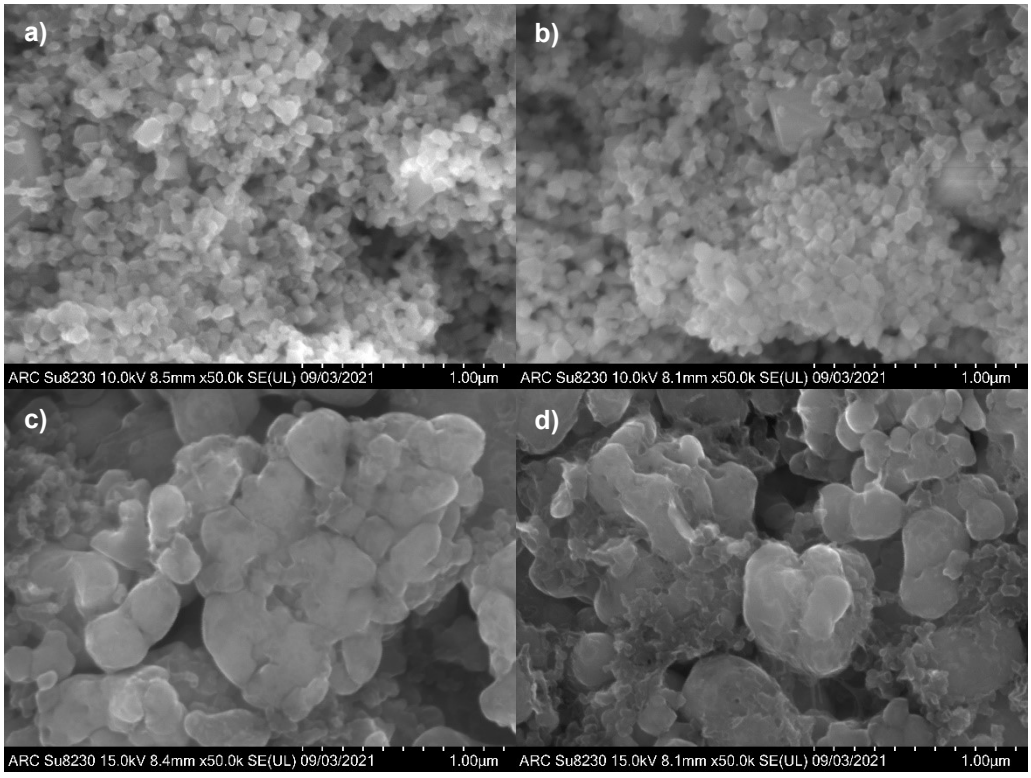

Figure S15: SEM images of a) LTO anode after 50 cycles at 0.5 C, b) 0.5 at 50 °C, c) LFP anode after 50 cycles at 0.5 C, and d) 0.5 C at 50 °C using LiTFSI DEE.